J. Fluid Mech. (1986), *vol.* 163, *pp.* 149–169
Printed in Great Britain

Vortex excitation of prisms with elongated rectangular, H and ⊢ cross-sections

By YASUHARU NAKAMURA
AND MASAMICHI NAKASHIMA
Research Institute for Applied Mechanics, Kyushu University, Kasuga 816, Japan

(Received 2 February 1985)

This is an experimental investigation of vortex excitation of prisms with elongated rectangular, H- and ⊢-shaped cross-sections, where the depth parallel to the flow is much greater than the height perpendicular to the flow. Measurements are made of free oscillations in a wind tunnel and flow visualizations in a water tank. The flow around elongated bluff prisms is dominated by the impinging-shear-layer instability where the separated shear layers become unstable in the presence of different kinds of shape of the rear part of the cross-section, which may include sharp trailing edges. The two unstable shear layers interact with each other when they meet together downstream of the prism, thereby forming Kármán vortices with the same frequency of oscillation. The former impinging-shear-layer instability is largely responsible for vortex excitation of elongated bluff prisms.

1. Introduction

Recently there has been increasing attention to wind-induced self-excited oscillations of long-span cable-stayed bridges with bluff cross-sections, especially those with edges that are higher than the central cross-section (figure 1). These excitations usually occur at relatively low wind speeds, say around 10 m s^{-1}, and the amplitudes of oscillation remain restricted and never grow up to destructive levels as often occurs with other types of excitations at high wind speeds. However, they can be one of the main sources of structural fatigue and vehicle unserviceability. The aerodynamic mechanism or mechanisms of these excitations must be elucidated if one wants to control or suppress them effectively.

Consider a two-dimensional bluff prism with a cross-section whose depth-to-height ratio is d/h, where d and h are the cross-section dimensions in the along- and cross-flow directions. For short prisms ($d/h \ll 1$), vortex excitation is presumably the most typical low-speed excitation. It can occur, often with beat modulations, in a very narrow range of wind speed centred on the one at which the structural frequency of a bluff prism coincides with that of the shedding of Kármán vortices.†

On the other hand, the flow around elongated prisms ($d/h \gg 1$) is quite different and is not yet understood, though it is known that vortex excitation still occurs. It is believed to be responsible for the excitations of the various structural modes of the old Tacoma Narrows Bridge in vertical translation and torsion that were observed prior to its destructive torsional flutter (Farquharson 1952). The bridge had a cross-section that was equivalent to an H-section with $d/h = 5.0$.

† In this paper Kármán vortices are defined as the flow instability where the two shear layers separated from a bluff body interact with each other and roll up to form discrete vortices.

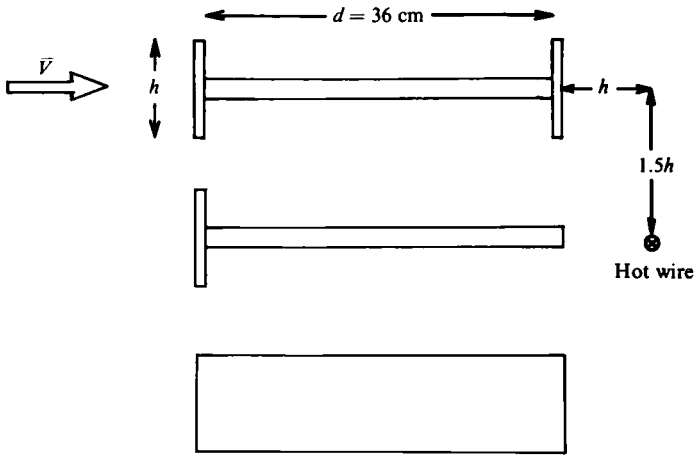

FIGURE 1. Sketch of the models used for excitation measurements.

By contrast, it is now known that many elongated bluff prisms can be excited in vertical translation or torsion at wind speeds well below the resonance one. For example, it was shown (Nakamura & Mizota 1975) that a rectangular prism with $d/h = 2.0$ can be excited in vertical translation at wind speeds around half the resonance one. The excitation was shown to grow up spontaneously from rest with little beat modulations.

Recently Komatsu & Kobayashi (1980) made unsteady pressure measurements together with flow visualizations for oscillating elongated bluff prisms, and showed how aerodynamic exciting forces can be generated as one or two of the motion-dependent leading-edge vortices roll up over the side faces of an elongated bluff prism. On this basis, they suggested that most low-speed excitations of elongated bluff prisms, including the H-section prism with $d/h = 5.0$, are not associated with Kármán vortices but caused directly by the motion-dependent leading-edge vortices. The concept of the excitation due to the motion-dependent leading-edge vortices was supported by Shiraishi & Matsumoto (1983) who recently compiled a number of previously published data on the low-speed excitations of bridge deck sections. However, it is in contrast to the general view that the low-speed excitations of the old Tacoma Narrows Bridge were due to Kármán vortices. It appears that no precise mechanism or mechanisms of the low-speed excitations of elongated bluff prisms have yet been identified.

The present paper is concerned with an experimental investigation into the low-speed excitations of bluff prisms with elongated H, ⊢ and rectangular cross-sections. The results of excitation measurements conducted in a wind tunnel and those of flow visualizations conducted in a water tank are presented and discussed.

2. Experimental arrangements and procedures

The experiment was divided into two parts. The first part of the experiment was conducted in a wind tunnel with a rectangular working section 3 m high, 0.7 m wide and 2 m long. It included excitation measurements on spring-supported models together with measurements of the frequency of Kármán vortices for models at rest.

As is shown in figure 1, the models used in the experiment had H, ⊢ and rectangular

cross-sections with depth-to-height ratios ranging from $d/h = 2.0$ to 5.0. They were 36 cm in depth, 65 cm in span and had 36 cm by 72 cm end plates. The basic structural member of the model was a 14 mm thick light plastic plate with metal backbones. H and ⊢ configurations were obtained by attaching 5 mm thick girder plates of light plastic to the basic member plate. Rectangular configurations were obtained by covering the basic member plate with plates of the same material with additional ribs. In some measurements, a 1.2 m long and 5.5 mm thick splitter plate was inserted downstream of the model.

The model was mounted horizontally in the working section and suspended by flexural and coil springs that were set up outside the working section to allow either vertical translation (figure 2*a*) or torsion about the model centre axis (figure 2*b*). The displacement of the model was detected by using strain gauges that were cemented on the surfaces of the flexural springs. Table 1 shows some sample values for the frequency of oscillation f_0 and the logarithmic damping δ_0 of the model in still air together with the Scruton number Sc that is defined by $Sc = 2m\delta_0/(\rho d^2)$ or $2I\delta_0/(\rho d^4)$, where ρ is the air density, and m and I are the mass and the moment of inertia of the model per unit span. The still-air damping in vertical translation was obtained for the system where only the basic member plate was mounted in the working section with the flat faces in the vertical direction. This was considered to be more representative of the structural damping than that for the normal system which included a significant aerodynamic contribution. The size of the model and the frequency of oscillation had to be large enough to observe low-speed excitations with sufficient accuracy. If they were very small, low-speed excitations would occur at very low wind speeds so that no reliable results would be obtained.

The experimental wind speed ranged from $V = 2$ to 12 m s^{-1}, approximately, so that the corresponding Reynolds number, based on the depth d, was approximately (5 to 30) $\times 10^4$. The frequency of regular vortex shedding for the model at rest was measured by a hot-wire anemometer where the probe was normally positioned $1h$ downstream of the model and $1.5h$ down the centreline (figure 1), from which the Strouhal number was determined. For the Strouhal-number measurement, small models with $d = 18$ cm having 54 cm by 72 cm end plates were also used. The thickness of the member plate for H- and ⊢-section prisms was 3 mm. The depth-to-height ratio of the small models ranged from $d/h = 1.0$ to 10.0.

The second part of the experiment was conducted in a water tank 0.4 m deep, 0.4 m wide and 10 m long. The flow visualization was made on H- and ⊢-section prisms with $d/h = 5.0$ by using a hydrogen-bubble method. The models were made of brass and had $d = 4$ cm, $h = 0.8$ cm and a span of 38 cm. The model was attached to a carriage, whose speed was adjusted to 4 cm s^{-1} in the experiment. The carriage was equipped with a mechanical vibrator that could give cross-flow oscillation to the model. The period of oscillation was varied from 0.86 to 2.50 s, approximately, and the amplitude of oscillation was constant and equal to $y_0 = 1.5$ mm $(= 0.19h)$ throughout the experiment.

Hydrogen bubbles were generated successively by means of an electronic pulse generator from a thin stainless-steel wire of 30 μm diameter that spanned just upstream of the model. The timelines of hydrogen bubbles could highlight the separated shear layers and the subsequent regular vortex shedding. The photographs were taken with a motor-driven camera that was mounted on the carriage with an exposure time of $\frac{1}{60}$ s. The shutter pulse of the camera and the signal of the model oscillation were pen-recorded simultaneously, from which the periods of regular vortex shedding and the model oscillation were determined.

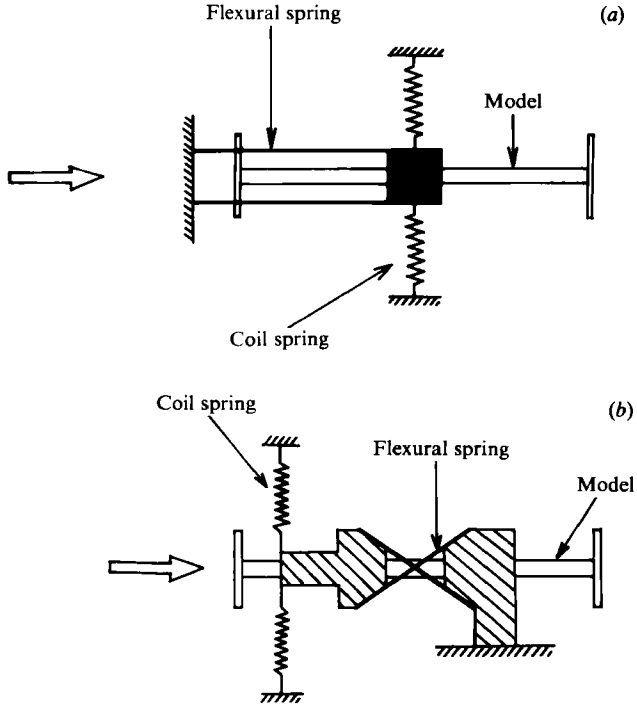

FIGURE 2. Model-support system. (*a*) Vertical translation; (*b*) torsion.

	f_0 (Hz)	δ_0	Sc
Vertical translation	6.75	0.005	0.17
Torsion	5.75	0.013	0.09

TABLE 1. Sample values for the frequency and logarithmic damping of the model in still air together with the Scruton number

3. Combined blockage and end effects

In an experiment using a sectional model with end plates the combined blockage and end effects should be considered. In the present experiment the most severe cases were those for the models with $d/h = 2.0$ that had a blockage ratio of 6%. It was expected that the effects would be decreased progressively with increasing d/h since the depth of the model was constant in the present experiment.

Figure 3 shows the effect of the size of rectangular end plates on the base-pressure coefficient of an H-section prism with $d/h = 2.0$ for two blockage ratios of 3 and 6%. With sufficiently large values of H/h, where H is the crossflow dimension of the end plate, the base-pressure coefficient was free from the end effects and only dependent on the blockage ratio. By assuming that the base-pressure coefficient decreases proportionally with the blockage ratio (Nakamura & Ohya 1984), the value of the base-pressure coefficient that is free from both the blockage and end effects is estimated as a dotted line.

The base-pressure coefficients of the large and small models used in the present

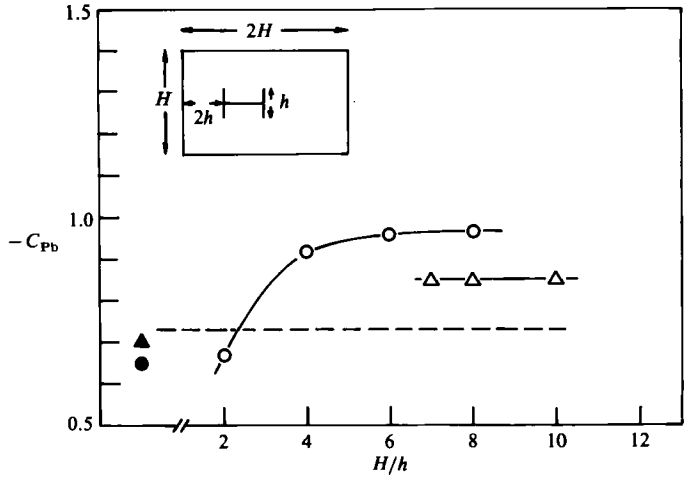

FIGURE 3. Effect of end-plate size on the base-pressure coefficient of an H-section prism with $d/h = 2.0$. ○, ●, blockage ratio 6%; △, ▲, 3%; ----, corrected for the blockage effect. Black symbols correspond to the models used for excitation and Strouhal-number measurements.

experiment are also shown as black symbols. They are seen to be fortuitously equal to the corrected value as a result of the combined blockage and end effects. On this basis no corrections were applied to the present experimental data.

4. Excitation of H-section prisms and the effects of a long splitter plate

Figures 4(*a*, *b*) show the low-speed excitations of an H-section prism with $d/h = 5.0$ in vertical translation and in torsion respectively. The abscissa indicates the experimental and the reduced wind speed, the latter of which is defined by $\bar{V} = V/(f_0 d)$. The white and black symbols in the figures indicate respectively the amplitude and the frequency of oscillation, while the straight line indicates the variation of the frequency of Kármán vortices with the wind speed for the model at rest. Figure 5 presents a sample record showing the growth of the excitation in vertical translation at $V = 2.2$ m s^{-1}.

As can be seen in figure 4(*a*, *b*), excitation often occurred in two different ranges of wind speed. It always had restricted amplitudes, but, in the case of the second excitation in torsion (figure 4*b*), only the initial phases were explored since further increase in amplitude would destroy the support system. The excitation often had hysteresis near the quench speed, as is shown by arrows in figure 4(*a*). That is, responses to increasing wind speed were often different from those to decreasing wind speed. For convenience, only responses to increasing wind speed are presented in the following figures.

Figure 4(*a*, *b*) shows that the second excitation, whether in vertical translation or in torsion, was vortex excitation since it started at around the resonance wind speed. This is in agreement with the general view about the low-speed excitations of the old Tacoma Narrows Bridge that was mentioned earlier.

Figure 6 shows the results of measurement for an H-section prism with $d/h = 2.0$ in vertical translation. In this case two different modes of vortex shedding were observed. Namely, there was a high-frequency mode (indicated by a full line) in addition to a low-frequency one (indicated by a dotted line). It is interesting that

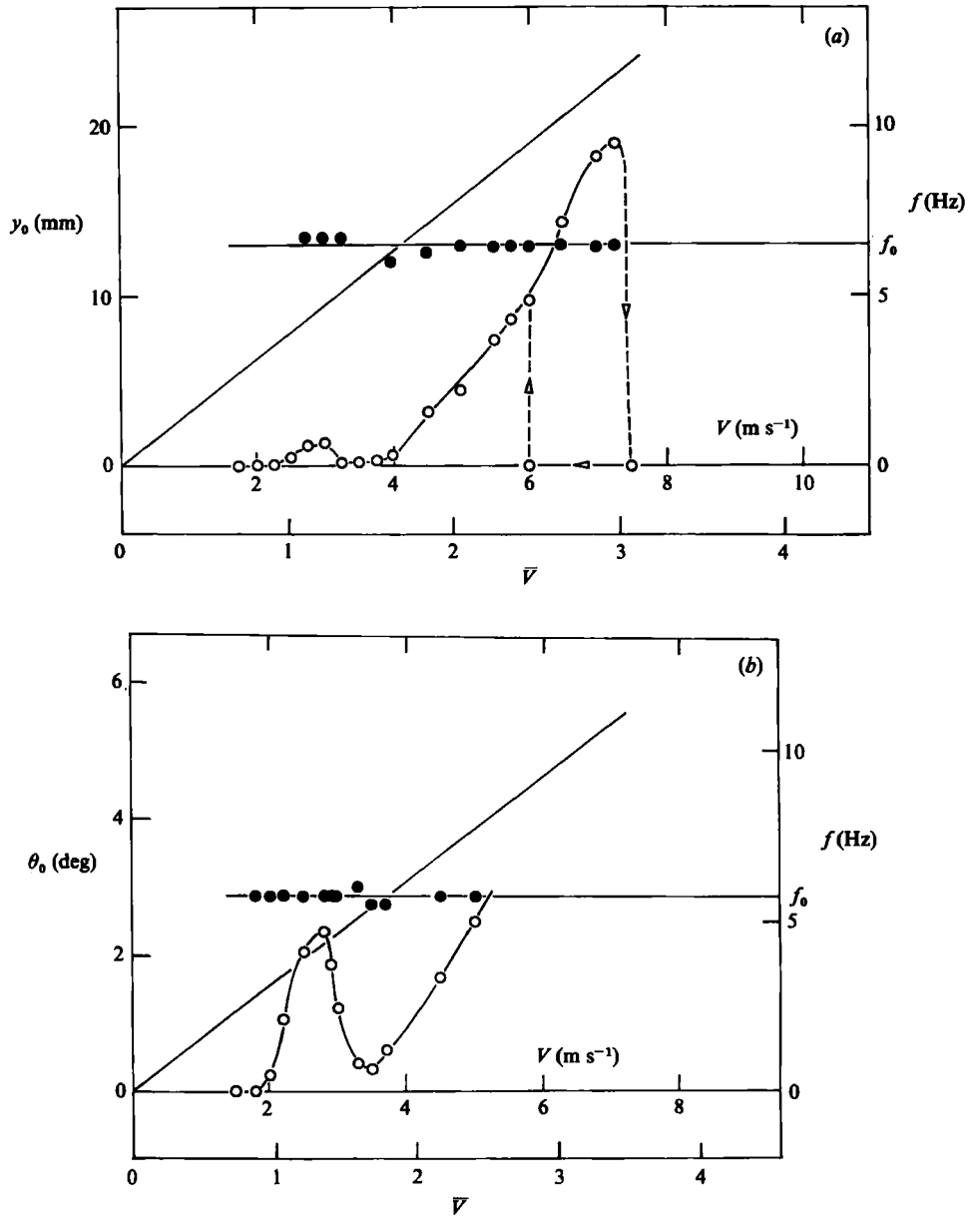

FIGURE 4. Low-speed excitations of an H-section prism with $d/h = 5.0$. ○, amplitude; ●, frequency; ——, frequency of Kármán vortices for the model at rest. (*a*) Vertical translation; (*b*) torsion.

the excitation started at the resonance wind speed that was associated with the high-frequency mode of vortex shedding. A similar result was obtained for torsional oscillations.

In order to get insight into the nature of the excitation, an experiment was designed in which a long splitter plate was inserted downstream of the spring-supported model and excitation was observed by varying the gap between the model and the splitter plate. The results are exemplified in figure 7 (*a*, *b*) for an H-section

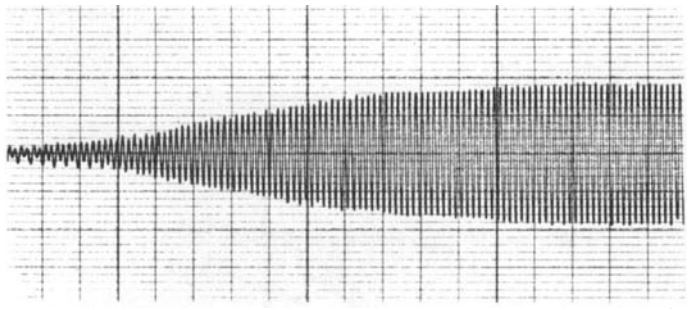

FIGURE 5. Time history of low-speed excitation. H-section prism with $d/h = 5.0$; vertical translation; $V = 2.2$ m s^{-1}.

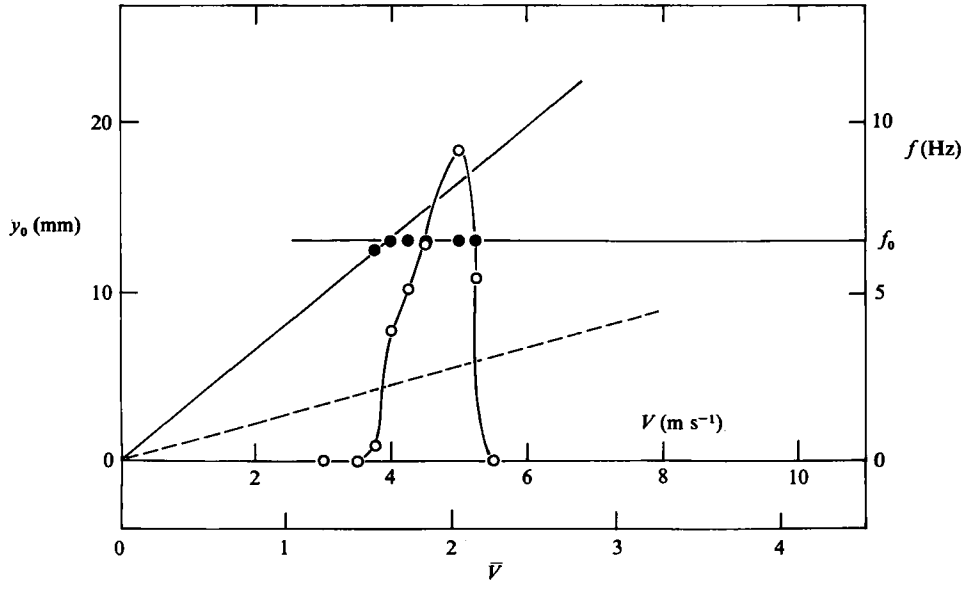

FIGURE 6. Low-speed excitation of an H-section prism with $d/h = 2.0$ in vertical translation. Symbols as in figure 4.

prism with $d/h = 4.0$ in vertical translation and that with $d/h = 2.0$ in torsion. It can be seen that the excitation started at the same wind speed as that for the prism without a splitter plate, with little modification in amplitude at its initial phase. In other words, the presence of a splitter plate did not affect the initial phase of the excitation. This appears to be puzzling for the following reasons.

Obviously, there are no Kármán vortices to be formed downstream of a prism with a splitter plate since the splitter plate now prevents the upper and lower separated shear layers from interacting with each other. It follows that the excitation would not be associated with Kármán vortices. On the other hand, the fact that excitation does start at the resonance wind speed suggests that there could be some substantial correlation between the excitation and Kármán vortices. Any correct explanation for the excitation must reconcile these two conflicting ideas.

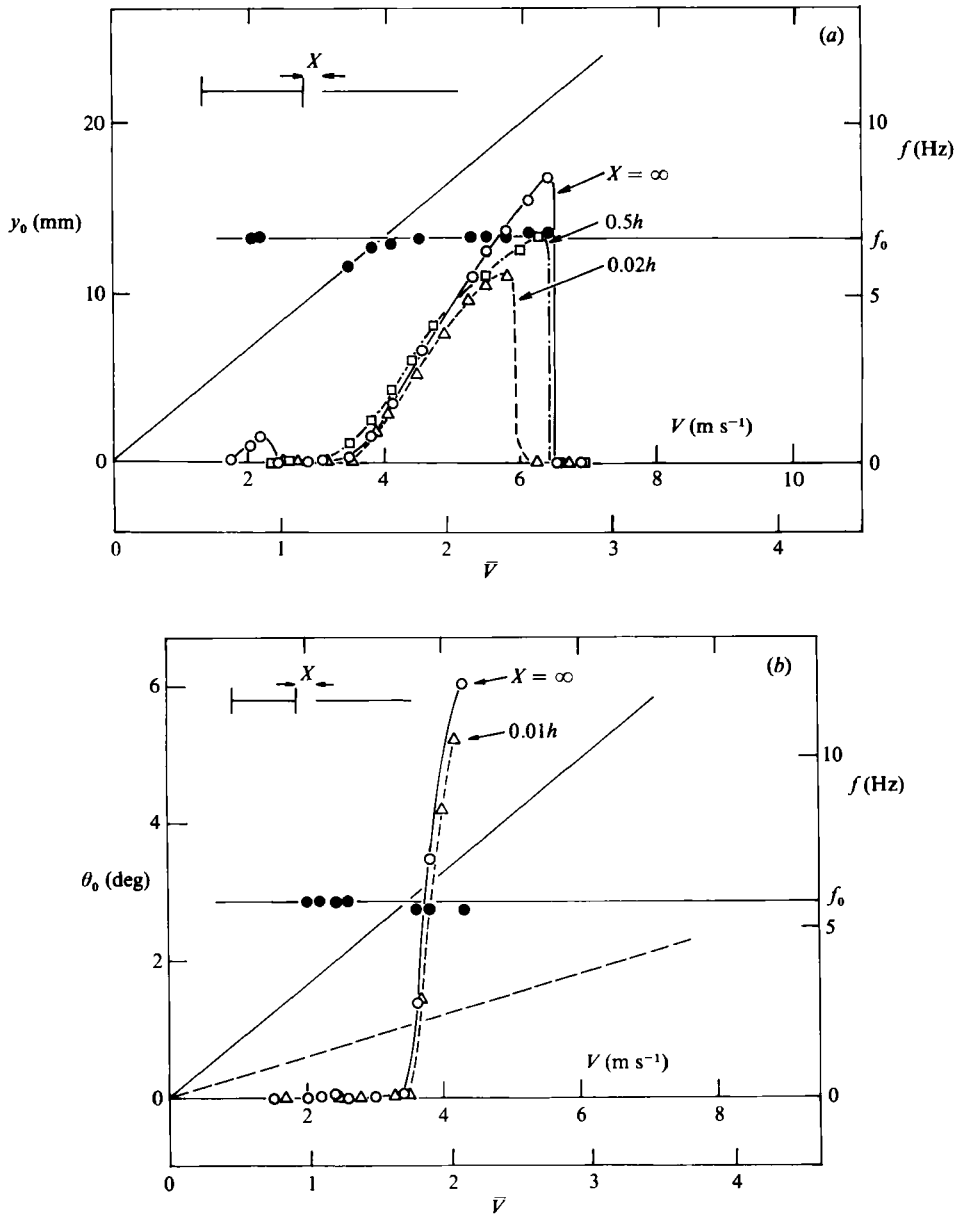

FIGURE 7. Effects of a long splitter plate on the low-speed excitations of H-section prisms. White symbols, amplitude; ●, frequency for $X = \infty$. (*a*) $d/h = 4.0$, vertical translation; (*b*) $d/h = 2.0$, torsion.

5. High-frequency mode of vortex shedding

Figure 8 summarizes the results of measurement for the Strouhal number $St(h)$ that is based on the height h for H-section prisms with various values of the depth-to-height ratio. Two examples of the hot-wire signal and its power spectrum are presented in figure 9(*a*, *b*). The values of the Strouhal number for the small ($d = 18$ cm) and the large ($d = 36$ cm) models in figure 8 are seen to agree with

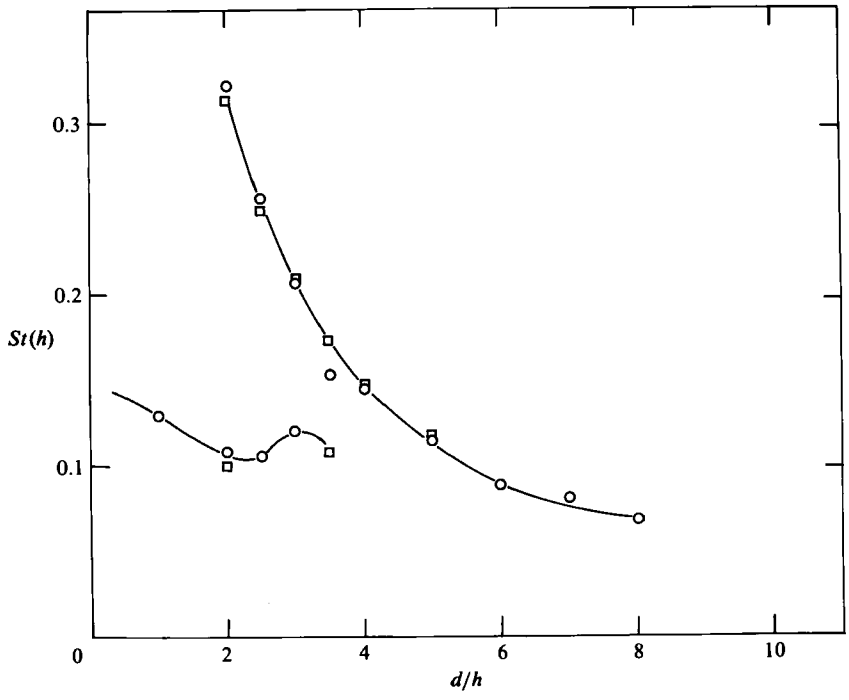

FIGURE 8. Strouhal number of H-section prisms. $St(h)$ is based on the prism height. ○, d = 18 cm; □, 36 cm.

each other, probably owing to the small combined interference effects that were discussed earlier.

It is seen that there are two modes of vortex shedding with different frequencies. With increase in d/h from zero, there is a transition from a low-frequency mode of vortex shedding to a high-frequency one, with an intermediate range between $d/h = 2.0$ and 3.5, approximately, where both modes were detected. In the transitional range it was sometimes difficult to specify dominant peaks in the spectrum because there were several such peaks. The high-frequency mode was observed over a wide range from $d/h = 2.0$ to 8.0. Beyond $d/h = 8.0$, no sharp peak was present in the spectrum, which indicated that the separated shear layers reattached somewhere on the sides.

Further attention will be focused on the high-frequency mode of vortex shedding and the related excitation. One essential key to the nature of the high-frequency vortex shedding may be obtained if one defines the Strouhal number $St(d)$ that is based on the depth d rather than the height h. This is shown in figure 10 where the Strouhal number of the high-frequency mode is almost constant and equal to 0.6 approximately over a wide range of d/h from 2.0 to 8.0.

6. Excitation coupled with the impinging-shear-layer instability

It is well known that the separated shear layer issuing from the upstream corner of a cavity often becomes unstable to roll-up in discrete vortices in the presence of the downstream corner. Such a flow instability, which belongs to a more general class of flow instabilities related to jets and wakes, is herein referred to as the impinging-

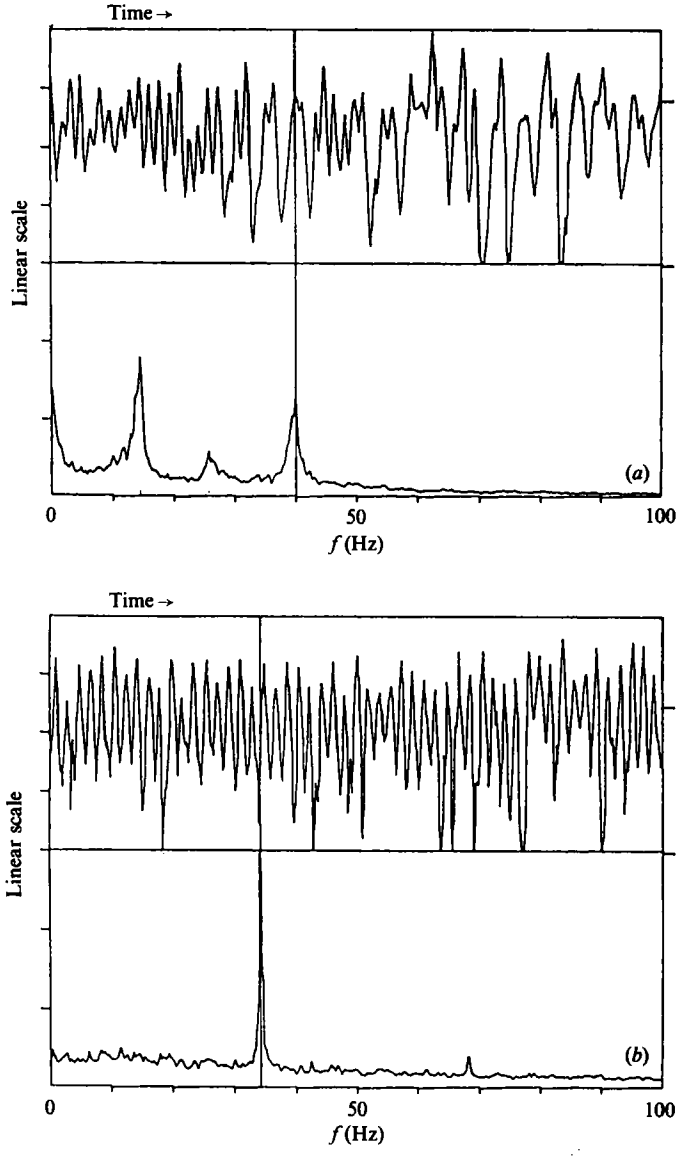

FIGURE 9. Time history and power spectrum of the hot-wire signal for H-section prisms at rest. $d = 18$ cm, $V = 11.0$ m s^{-1}. (*a*) $d/h = 2.0$; (*b*) $d/h = 5.0$.

shear-layer instability (Rockwell & Naudascher 1978). It is a single-layer flow instability in contrast to Kármán vortices, a double-layer flow instability. The frequency of vortex shedding of the instability is dependent on the flow speed and the cavity geometry together with the characteristics of the upstream boundary layer. For the turbulent shallow-cavity flow, the Strouhal number $St(d) = fd/V$, where f is the frequency of vortex shedding and d is the cavity length, is often constant and equal to 0.6 approximately, and hence independent of the cavity depth and width (Rockwell & Naudascher 1978).

It can be considered that an H-section consists of two cavities with a bottom plate in common. On this basis, it may be possible that the impinging-shear-layer

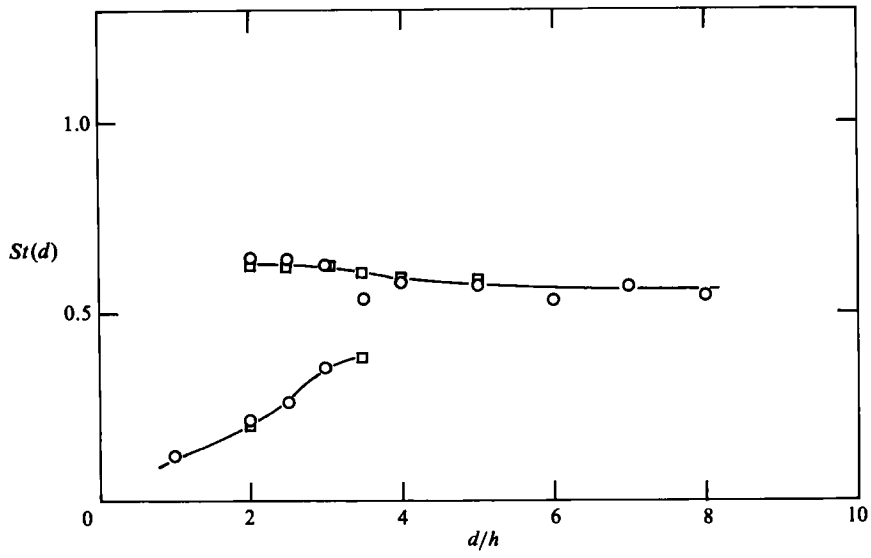

FIGURE 10. Strouhal number of H-section prisms. $St(d)$ is based on the cylinder depth. Symbols as in figure 8.

instability would occur for the flow past an H-section prism. Namely, the separated shear layers on the upper and lower sides may be unstable in the presence of the sharp trailing edges. The two unstable shear layers are basically independent, but, once they meet together downstream of the prism, they can interact with each other and be formed as Kármán vortices.

It is suggested that the high-frequency mode of vortex shedding of an H-section prism having the Strouhal number roughly equal to 0.6 for a wide range of d/h, is Kármán vortices of a special type, that is, Kármán vortices that are associated with the impinging-shear-layer instability. When a splitter plate is inserted downstream of an H-section prism, the upper and lower shear layers can no longer interact so that no Kármán vortices can be formed. However, it is possible for the impinging-shear-layer instability to remain with approximately the same frequency as that of Kármán vortices. This is why the aeroelastic excitation of an elongated H-section prism with a splitter plate can occur at the resonance wind speed corresponding to the one without a splitter plate. Figure 11 shows the spectrum of the hot-wire signal for an H-section prism with $d/h = 5.0$ with a long splitter plate. The hot-wire probe was positioned $1d$ downstream of the trailing edge and $1.8h$ away from the splitter plate. The arrow in the figure shows the frequency of the sharp peak for the prism without a splitter plate. Although the spectrum is broad-banded, it indicates the presence of the impinging-shear-layer instability.

It is shown (Ziada & Rockwell 1982) that the impinging-shear-layer instability for a cavity has higher harmonics in addition to the fundamental mode. The impinging-shear-layer instability for an H-section prism may also have higher harmonics so that the Strouhal number $St(d)$ be given by $0.6n$, where n is a positive integer. Similarly, the aeroelastic excitation may have higher harmonics.

Figure 12 summarizes the results of the excitation measurement for an H-section prism for various values of d/h. Here, the reduced onset wind speeds for vertical translation and torsion are plotted against d/h together with $\overline{V}_{cr}$ and $\frac{1}{2}\overline{V}_{cr}$ that represent the inverses of the Strouhal number for the high-frequency mode of vortex

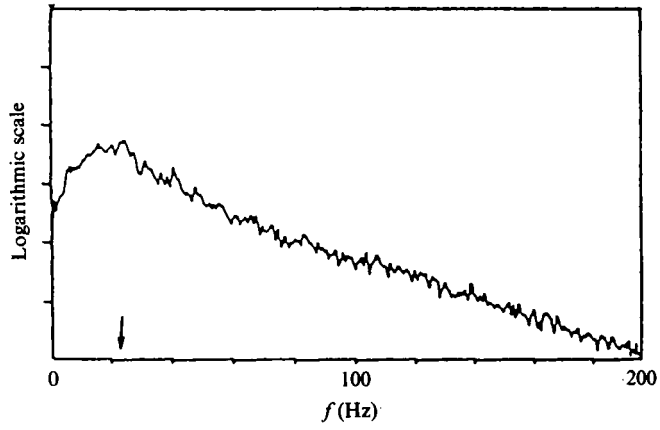

FIGURE 11. Power spectrum of the hot-wire signal for an H-section prism with $d/h = 5.0$ with a long splitter plate. $V = 6.7$ m s^{-1}; the arrow indicates the sharp peak for the same prism without a splitter plate.

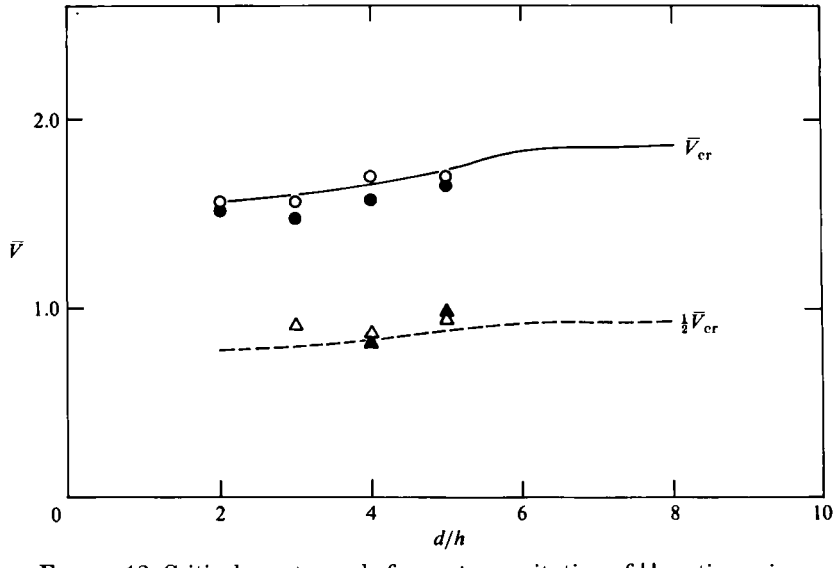

FIGURE 12. Critical onset speeds for vortex excitation of H-section prisms. ●, ▲, vertical translation; ○, △, torsion.

shedding and its first harmonic. The correlation between the excitation and the impinging-shear-layer instability is found to be excellent.

The term vortex excitation has been used specifically for the excitation due to Kármán vortices in the present paper. However, it can include a more general class of aeroelastic excitations that are associated with flow instabilities. In particular, it can include the excitation due to the impinging-shear-layer instability.

7. Flow visualization of H-section prisms

Figure 13(*a*) shows the flow pattern of an H-section prism with $d/h = 5.0$ at rest that was obtained in a water tank using a hydrogen-bubble method, while figure 13(*b*) shows that for the prism with a splitter plate of $4d$ in length. The value of the Reynolds number was about 1200 with $d = 4$ cm and $V = 4$ cm s^{-1}.

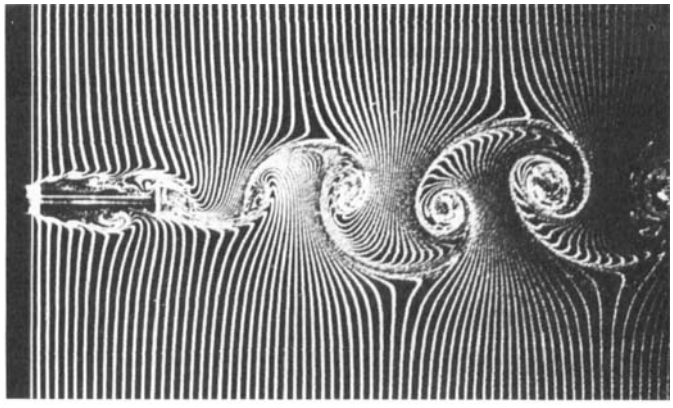

(*a*)

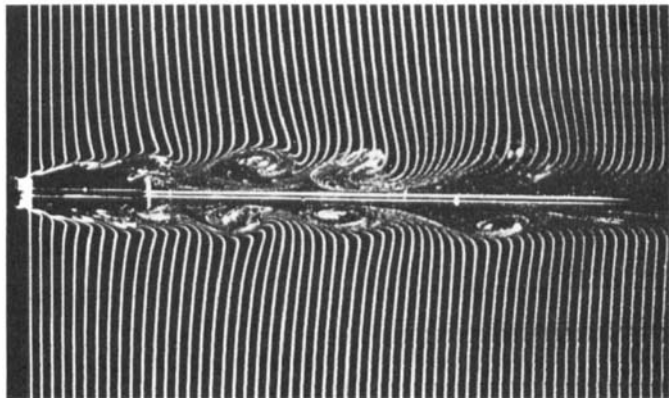

(*b*)

FIGURE 13. Flow around an H-section prism with $d/h = 5.0$ at rest. $d = 4$ cm; $V = 4$ cm s^{-1}; $R = 1200$; hydrogen-bubble method is used. (*a*) Prism without a splitter plate; (*b*) prism with a splitter plate.

As is shown in figure 13(*a*), very regular Kármán vortices were formed behind the prism. The period of shedding was found to be $T_0 = 1.86$ s so that the Strouhal number of 0.54 was obtained, a value that is comparable to the wind-tunnel measurement of 0.6 despite large differences in Reynolds numbers. The flow pattern also suggests the presence of the impinging-shear-layer instability. Namely, the separated shear layers issuing from the leading edges are seen to roll up and escape past the trailing edges cyclically before being organized as Kármán vortices in the downstream.

More direct evidence of the impinging-shear-layer instability is given by figure 13(*b*), where roll-up of the shear layers and subsequent escape past the trailing edges are also seen, although shedding was found to be less regular with sporadic intervals of irregularity. Although shedding of vortices on the two sides was

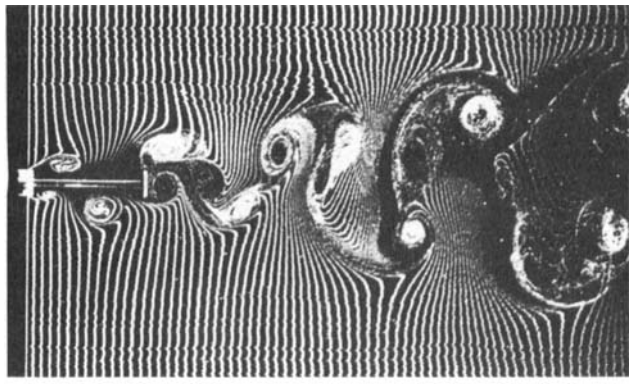

(*a*)

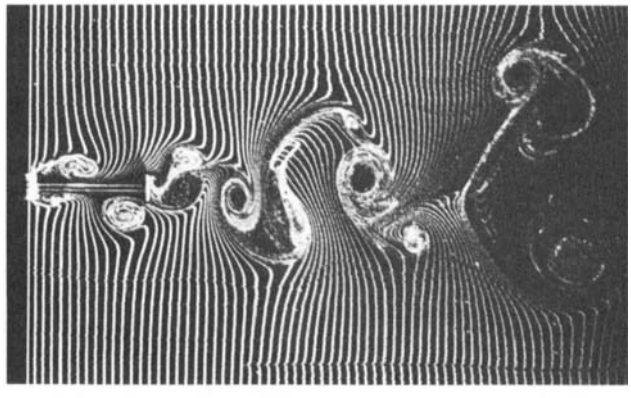

(*b*)

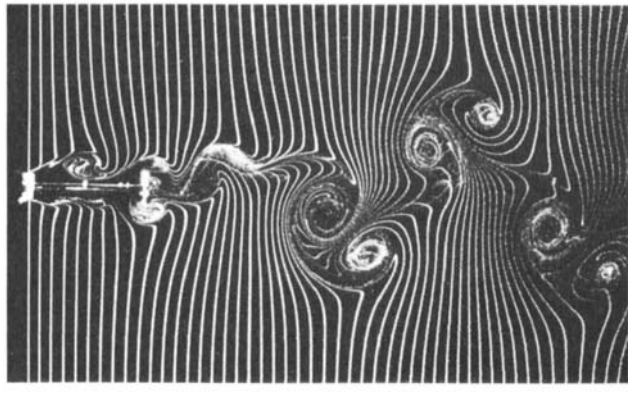

(*c*)

FIGURE 14. Flow around an H-section prism with $d/h = 5.0$ in vertical translation. $d = 4$ cm; $V = 4$ cm s^{-1}; $R = 1200$; oscillation amplitude, 1.5 mm ($= 0.19h$). Photographs correspond to the instant when the prism is at the extreme downward position. (*a*) $T = 1.73$ s; (*b*) $T = 1.86$ s (equal to the period of natural shedding); (*c*) $T = 2.50$ s.

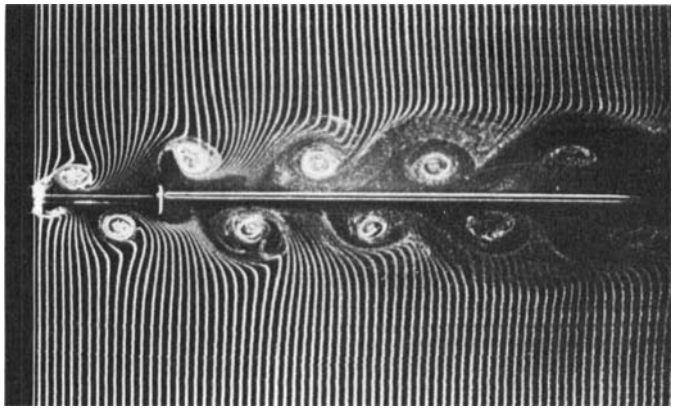

FIGURE 15. Flow around an oscillating H-section prism with $d/h = 5.0$ with a splitter plate. Flow conditions are the same as in figure 14(*a*).

not in antiphase but rather in phase, the period of shedding was found to be the same as that for the prism without a splitter plate shown in figure 13(*a*).

Figure 14(*a–c*) shows the flow patterns of an H-section prism with $d/h = 5.0$ oscillating in vertical translation with an amplitude of 1.5 mm ($= 0.19h$) and periods of $T = 1.73$, 1.86 (equal to that of the natural shedding) and 2.50 s, respectively. The numerical values of the period coincide with those of the reduced flow speed since $d = 4$ cm and $V = 4$ cm s^{-1}. The three photographs shown all correspond to the instant when the cyclinder was at the extreme downward position.

One can see that strong vortices were shed from the leading edges of the prism in synchronism with the prism motion and the flow downstream of the prism was completely locked in with it. It is also seen that increasing the period of oscillation caused shed vortices to rapidly change their positions relative to the side faces. The effects of a splitter plate is shown in figure 15 where the period of oscillation was $T = 1.73$ s and hence one can compare the flow pattern with that of figure 14(*a*). It is surprising that the behaviour of the motion-dependent vortices on the prism sides is very similar for the two cases, although the flows downstream of the prism are very different.

Incidentally, figure 14(*a–c*) shows that the escaping vortex induces a secondary vortex on the opposite side and these two are shed as a pair of mushroom-type vortices. The secondary vortices were observed earlier by Shiraishi & Matsumoto (1983). It would be characteristic of an elongated sharp-edged bluff prism because the photographs of an oscillating circular cylinder (Koopman 1967) do not indicate such secondary vortices. However, the role played by the secondary vortices in vortex excitation should not be exaggerated because, as figure 15 shows, no such vortices were observed for an oscillating prism with a splitter plate.

Figure 16(*a*, *b*) presents another comparison of the flow patterns for prisms with and without a splitter plate. The period of oscillation was equal to 0.86 s, a value approximately half that of the natural shedding, and hence the flow corresponds to the first-harmonic excitation. Again, the flow patterns over the prism sides in the two cases are surprisingly similar, despite large difference in those behind the prism. Another point of interest relative to figure 16(*a*) is that, although the prism was oscillating at about $\frac{1}{2}T_0$, the wake downstream of the prism was reorganized with the

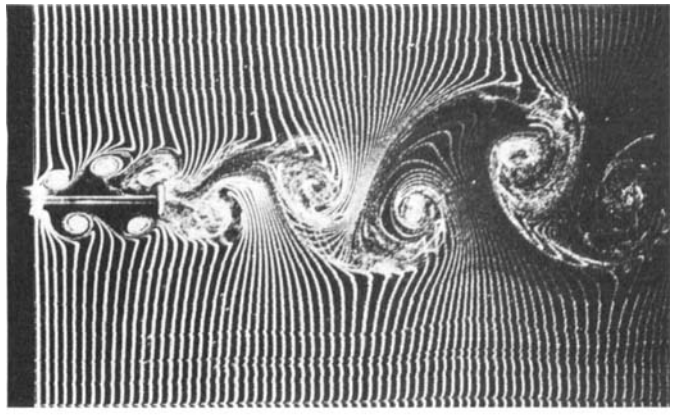

(a)

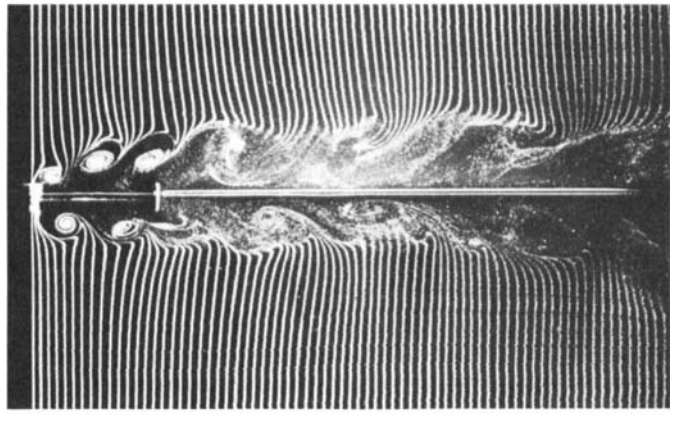

(b)

FIGURE 16. Flow around an H-section prism with $d/h = 5.0$ in vertical translation at $T = 0.86$ s. $d = 4$ cm; $V = 4$ cm s^{-1}; $R = 1200$. (a) Prism without a splitter plate; (b) prism with a splitter plate.

period of T_0, i.e. that of the natural shedding itself. It appears that the reorganization of the wake would be critical at $\frac{1}{2}T_0$, but this was not confirmed in the present experiment.

8. The results for ⊢-section and rectangular prisms

The experimental results for ⊢-section and rectangular prisms showed no substantial difference from those for H-section prisms. Figure 17 (*a*, *b*) presents the variations of the Strouhal number with d/h for ⊢-section and rectangular prisms respectively. In figure 17 (*b*) the measurements by Okajima, Sugitani & Mizota (1982) are also shown for comparison. The impinging-shear-layer instability occurs over a

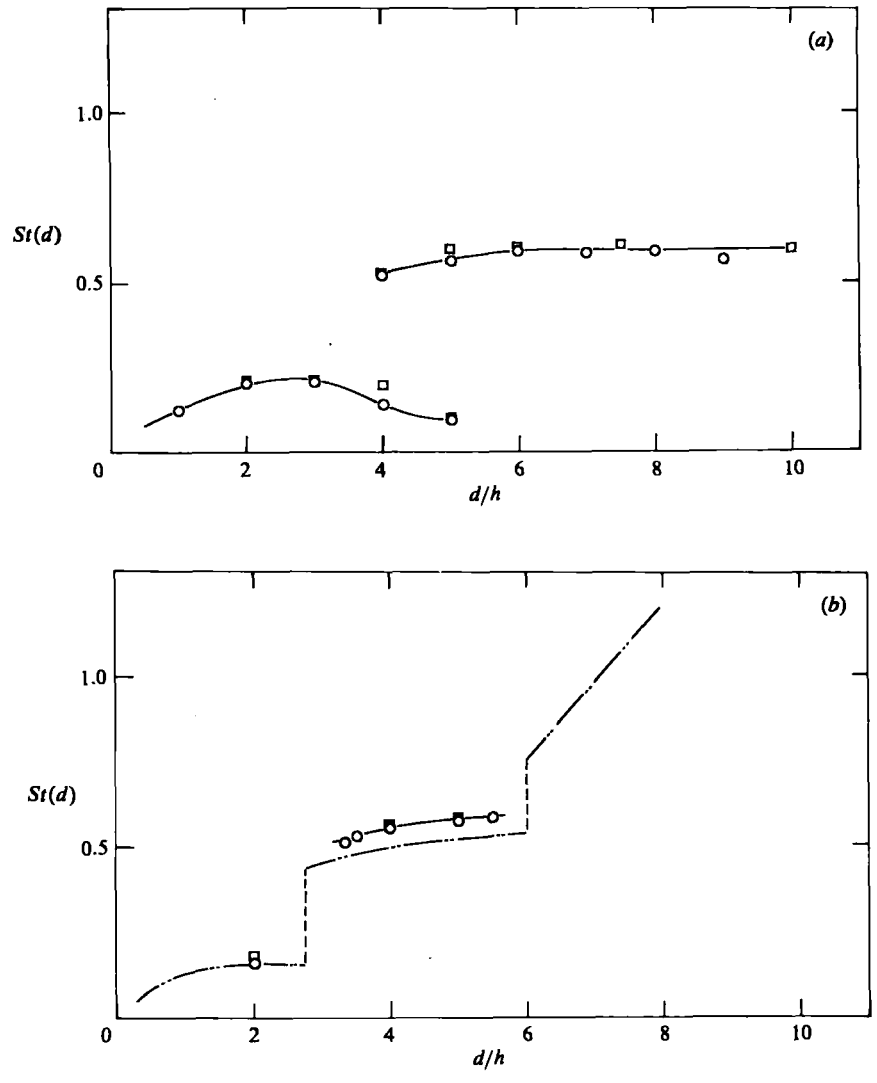

FIGURE 17. Strouhal number *vs.* depth-to-height ratio. $St(d)$ is based on the prism depth. (*a*) ⊢-section prism: (*b*) Rectangular prism; ——·——, Okajima, Sugitani & Mizota (1982).

wide range from $d/h = 4.0$ to 10 for ⊢-section prisms (figure 17*a*), while it is restricted to a narrow range from $d/h = 3.0$ to 6.0 for rectangular prisms (figure 17*b*). Okajima, Sugitani & Mizota (1982) commented that the second and the third modes of vortex shedding in figure 17(*b*) indicate respectively the intermittent and the steady reattachment of the shear layers on the sides. Their comment is compatible with the present concept of the impinging-shear-layer instability.

Figure 18(*a*, *b*) summarizes the results of the excitation measurement. Supplementary results for a ⊢-section prism with $d/h = 7.5$ and a rectangular prism with $d/h = 6.0$, both in vertical translation, are also included in the figures. It is indicated that the excitation and the impinging-shear-layer instability are well correlated for these two types of bluff prisms. Excitation is also seen to occur for short prisms for which the hot-wire signals did not indicate sharp spectra for the

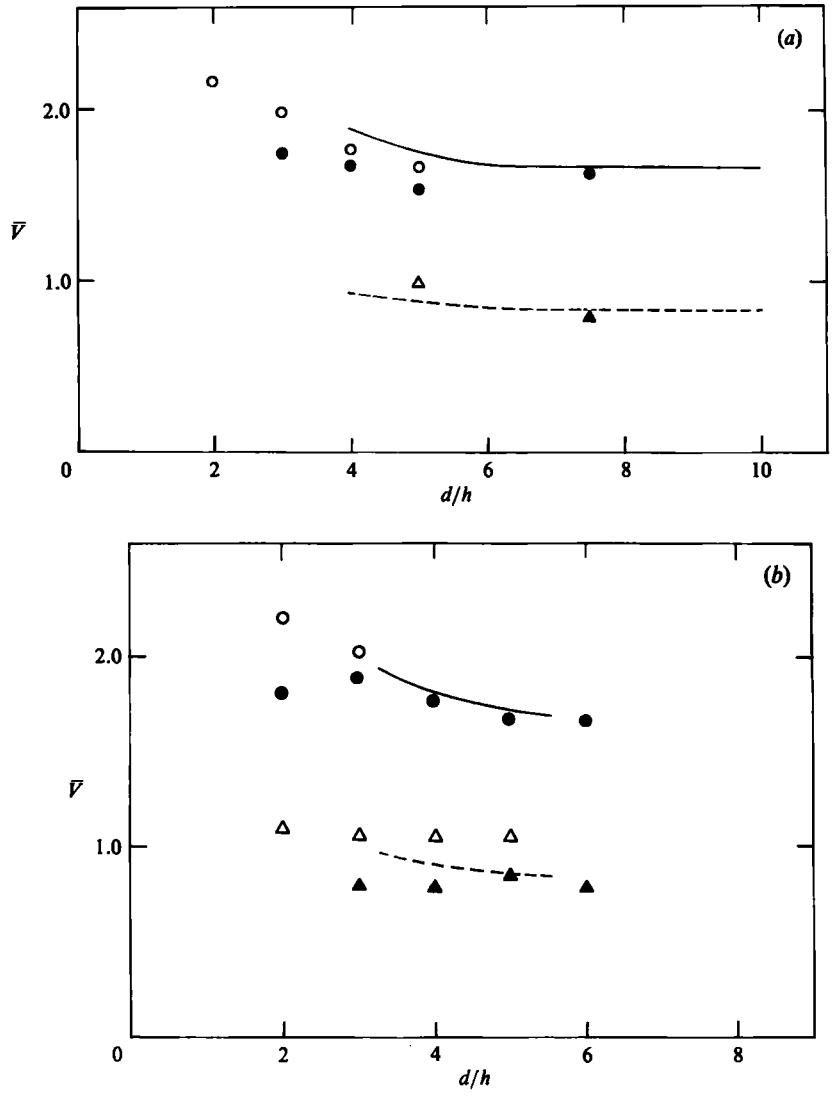

FIGURE 18. Critical onset speeds for vortex excitation. Symbols as in figure 12. (*a*) ⊢-section prism; (*b*) rectangular prism.

impinging-shear-layer instability. However, there is no doubt from the experimental trends that the observed excitations were associated with the impinging-shear-layer instability. One deviation from the general trend is that for rectangular prisms with $d/h = 4.0$ and 5.0 in torsion, only the first harmonic but no fundamental mode was excited.

Figure 19(*a*, *b*) shows the flow patterns for a ⊢-section prism with $d/h = 5.0$ at rest at two different instants. The flow conditions were the same as shown earlier. The two photographs indicate how the escaping upper vortex entrained the lower separated shear layer. Figure 19(*c*) shows the flow pattern for the prism oscillating in vertical translation with a period of 1.86 s, which was approximately equal to that of the natural shedding. The flow pattern is very similar to that for an oscillating H-section prism shown in figure 14(*b*).

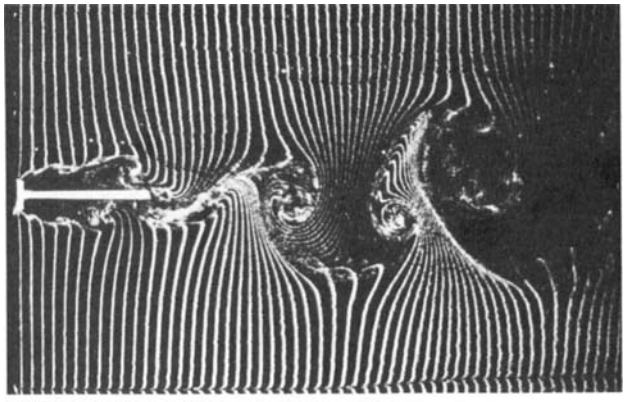

(*a*)

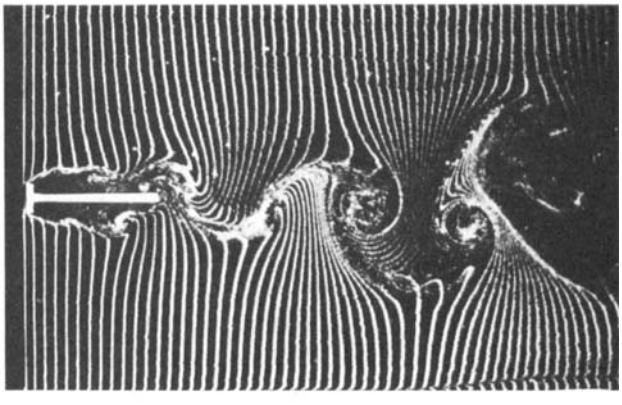

(*b*)

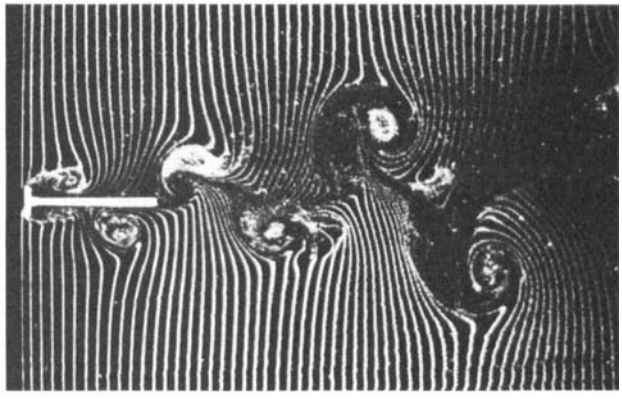

(*c*)

FIGURE 19. Flow around a ⊢-section prism with $d/h = 5.0$. $d = 4$ cm; $V = 4$ cm s^{-1}; $R = 1200$. (*a*), (*b*) Prism at rest; (*c*) prism in vertical translation at $T = 1.86$ s.

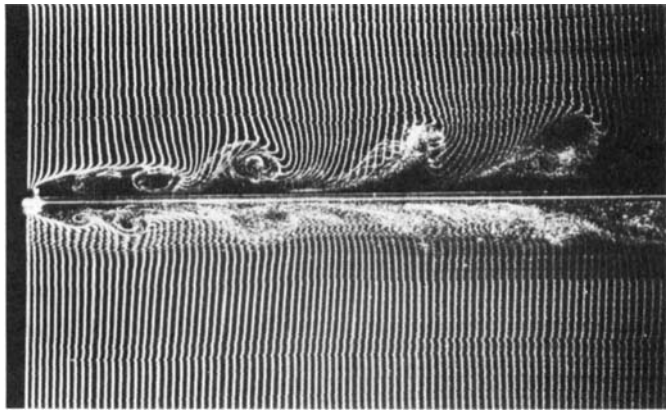

FIGURE 20. Flow around a very much elongated ⊢-section prism. $h = 8$ mm; $V = 4$ cm s^{-1}.

9. Some remarks on the separated-and-reattaching flow

Recent observations by Cherry, Hillier & Latour (1983, 1984) and Kiya & Sasaki (1984) showed that the separated-and-reattaching flow is not always steady but has vortex shedding of weak periodicity. The Strouhal number has a value of about 0.7 if it is based on the mean reattachment length L_R (Cherry *et al.* 1983). The flow past a very much elongated ⊢-section prism is an example of the separated-and-reattaching flow. It is interesting that shallow cavities, elongated bluff prisms with and without a splitter plate and a very much elongated ⊢-section prism all have the same Strouhal number of about 0.6 to 0.7. It is suggested that the impinging-shear-layer instability would also be responsible for the weak vortex shedding of a very much elongated ⊢-section prism. If a fence is introduced a distance d downstream of the leading edge of a very much elongated ⊢-section prism, the impinging-shear-layer instability would be controlled by the fence and the Strouhal number that is based on the depth d instead of L_R would become constant and equal to 0.6 approximately.

Periodic vortex shedding behind a very much elongated ⊢-section prism at a low Reynolds number is shown in figure 20 where the flow conditions were the same as those in figure 13(*b*). As the mean reattachment length was difficult to estimate, the Strouhal number based on the height h was determined and equal to $St(h) = 0.10$. This can be compared to the high Reynolds-number value of 0.08 if $L_R = 8.8h$ is assumed (Cherry *et al.* 1983). It should be added that, even at such a low Reynolds number, vortex shedding was often irregular and regular phases were less frequently observed.

10. Conclusions

The separated shear layers on the upper and lower sides of an elongated bluff prism can be unstable in the presence of sharp trailing edges. The instability has been referred to as the impinging-shear-layer instability in the present paper. The two unstable shear layers interact with each other when they meet together downstream of the prism, thus forming Kármán vortices with the same frequency of oscillation. The Strouhal number of vortex shedding is roughly constant and equal to 0.6 if it is based on the prism depth. Structures with elongated bluff cross-sections with and without a splitter plate are susceptible to the vortex excitation that is coupled with

the impinging-shear-layer instability. The impinging-shear-layer instability is one of the basic flow phenomena related to shallow cavities, elongated bluff prisms with and without a splitter plate and a very much elongated ⊢-section prism with a separated-and-reattaching flow.

We thank Messrs K. Watanabe, K. Sugitani and A. Nagano for their assistance in conducting the experiment. This work was supported in part by a grant from the Ministry of Education, Science and Culture of Japan.

REFERENCES

CHERRY, N. J., HILLIER, R. & LATOUR, M. E. H. 1983 *J. Wind Engng Indust. Aero.* **11**, 95–105.
CHERRY, N. J., HILLIER, R. & LATOUR, M. E. M. 1984 *J. Fluid Mech.* **144**, 13–46.
FARQUHARSON, F. B. 1952 *Bulletin Univ. Washington Engng Exp. Sta.* **116**, Part III.
KIYA, M. & SASAKI, K. 1984 *Bull Japan Soc. Mech. Engnrs* **50**, 1483–1490 (in Japanese).
KOMATSU, S. & KOBAYASHI, H. 1980 *J. Wind Engng Indust. Aero.* **6**, 335–362.
KOOPMAN, G. H. 1967 *J. Fluid Mech.* **28**, 501–512.
NAKAMURA, Y. & MIZOTA, T. 1975 *Proc. ASCE J. Engng Mech. Div.* **101**, EM6, 855–871.
NAKAMURA, Y. & OHYA, Y. 1984 *J. Fluid Mech.* **149**, 255–273.
OKAJIMA, A., SUGITANI, & MIZOTA, T. 1982 *Flow Visualization* **2**, Suppl., 71–74 (in Japanese).
ROCKWELL, D. & NAUDASCHER, E. 1978 *Trans. ASME* I: *J. Fluids Engng* **100**, 152–165.
SHIRAISHI, N. & MATSUMOTO, M. 1983 *J. Wind Engng Indust. Aero.* **14**, 419–430.
ZIADA, S. & ROCKWELL, D. 1982 *J. Fluid Mech.* **124**, 307–334.